Preparation and Characterization of Hollow Fiber Carbon Membranes from Cellulose Acetate Precursors

ARTICLE *in* INDUSTRIAL & ENGINEERING CHEMISTRY RESEARCH · JANUARY 2011

Impact Factor: 2.59 · DOI: 10.1021/ie101978q

4 AUTHORS, INCLUDING:

Xuezhong He
Norwegian University of Science and Techno…
31 PUBLICATIONS **628** CITATIONS
SEE PROFILE

Edel Sheridan
SINTEF
12 PUBLICATIONS **91** CITATIONS
SEE PROFILE

May-Britt Hägg
Norwegian University of Science and Techno…
97 PUBLICATIONS **1,496** CITATIONS
SEE PROFILE

I&EC research
Industrial & Engineering Chemistry Research

ARTICLE

pubs.acs.org/IECR

Preparation and Characterization of Hollow Fiber Carbon Membranes from Cellulose Acetate Precursors

Xuezhong He,[†] Jon Arvid Lie,[†] Edel Sheridan,[‡] and May-Britt Hägg[†,*]

[†]Department of Chemical Engineering, Norwegian University of Science and Technology, N-7491 Trondheim, Norway

[‡]Materials and Chemistry, SINTEF, Richard Birkelands vei 2, N-7034 Trondheim, Norway

ABSTRACT: Hollow fiber carbon membranes (HFCMs) were prepared from deacetylated cellulose acetate precursors using a multidwell carbonization protocol. FTIR, scanning electron microscopy, and thermogravimetric analysis−mass spectrometry were employed to characterize the HFCMs. Gas permeation tests were conducted with single gases (H_2, CO_2, N_2, and CH_4) as well as gas mixtures. The single-gas test results indicated that the molecular sieving mechanism dominated in the carbon membrane separation process. The effects and feed pressure on the carbon membrane performance were also investigated. Moreover, the gas-mixture test results indicated that the permeability and selectivity need to be optimized by adjusting the operating conditions (basically temperature) for the membrane process. The aging test result indicates that the permeability of the carbon membrane will decrease over time when it is exposed to the laboratory air.

1. INTRODUCTION

Membrane separation technology has become an increasingly attractive and competitive method of gas separation due to high performance, energy efficiency, and low economic costs. Carbon membranes are readily prepared by the carbonization of polymeric precursors and show promising results in gas separations, especially for CO_2 removal from natural gas/biogas and flue gas, oxygen enrichment of air, and purification of H_2. Fuertes et al. reported that carbon molecular sieve membranes have a potential to push the upper boundary of the permeability vs permselectivity trade-off relationship.[1] Up until now, different precursor materials such as polyimide,[2−4] polyacrylonitrile (PAN),[5] phenolic resin,[6] poly(phthalazinone ether sulfone ketone),[7] poly(phenylene oxide),[8,9] and cellophane paper[10] have been utilized for the fabrication of carbon membranes. The properties of the precursor will affect the carbon membrane performance and stability. Therefore, a suitable polymeric material should be chosen for the preparation of carbon membranes. Moreover, from the standpoint of large-scale application of most membrane materials, the hollow fiber geometry will be preferable to spiral-bound membranes because of the high packing density (membrane area per unit volume of the vessel) and easy module assembly. Strong interest has been shown in the preparation of hollow fiber carbon membranes (HFCMs) for gas separation recently,[11−16] based on improved selectivity and improved thermal, mechanical, and chemical stability compared to those of polymeric membranes already in use.

This work was focused on the investigation of the preparation and characterization of hollow fiber carbon membranes based on a cellulose acetate (CA) precursor, which is considered as one of the most suitable materials due to its commercial availability, low cost, and process ease.[17,18] The hollow fiber membranes were spun by the dry−wet hollow fiber spinning of a cellulose acetate precursor.[19,20] The prepared fibers were subsequently deacetylated with NaOH solution.[21,22] The high-performance HFCMs were prepared from the deacetylated hollow fibers by controlling the carbonization procedure using a specific protocol. The effects of different deacetylation conditions on the separation performance of the resulting HFCMs were examined in detail. In addition, the weight loss, structure, and morphology of the prepared carbon membranes were characterized by thermogravimetric analysis−mass spectrometry (TGA−MS) and scanning electron microscopy (SEM). The effects of the operating parameters such as the temperature and pressure on the gas separation performance and transport mechanism were also discussed on the basis of gas permeation tests. Finally, the aging of the hollow fiber carbon membrane was examined over time to investigate the durability of the carbon membrane.

2. EXPERIMENTAL SECTION

2.1. Materials. The polymer precursor material CA (MW 100 000) with an average acetyl content of 39.8% (degree of substitution (DS) of 2.45) was purchased from ACROS. Poly(vinylpyrrolidone) (PVP K10) was supplied by Sigma. The solvent *N*-methyl-2-pyrrolidone (NMP; >99.5%) was purchased from Merck (Darmstadt, Germany), and NaOH (>99%) used for deacetylation was also supplied by Merck. The materials were used as supplied without further purification.

2.2. Preparation of the Polymer Precursor. The spinning dope solution consisting of CA/PVP/NMP (22.5%/5%/72.5%) was prepared by the following procedure.[20] First, the solvent NMP and the additive PVP K10 were well mixed by mechanical stirring. The polymer CA was then added gradually into the mixture, after which the mixture was stirred for 24 h to ensure a homogeneous dope solution. The hollow fiber membranes were

Received: September 27, 2010
Accepted: December 21, 2010
Revised: November 29, 2010
Published: January 12, 2011

dx.doi.org/10.1021/ie101978q | *Ind. Eng. Chem. Res.* 2011, 50, 2080–2087

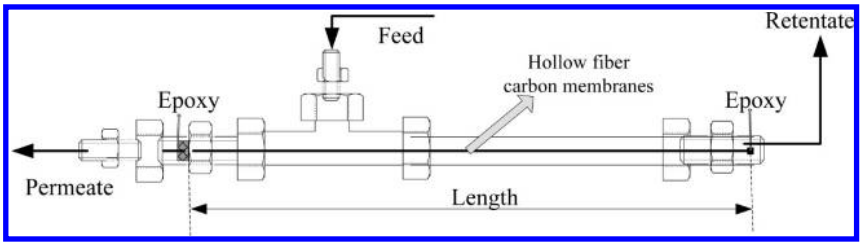

Figure 1. Schematic of the carbon membrane module.

spun using the well-known dry−wet spinning method. The dope solution and bore fluid were fed into the spinneret by gearwheel pumps. The optimal condition with an air gap of 25 mm, a dope flow rate of 2.2 mL/min, a bore fluid composition of water + NMP (85%), a bore flow rate that was 40% of the dope flow rate, and a water quench bath maintained at 50 °C was controlled for the whole spinning process. Following hollow fiber spinning, the fibers were placed in a water bath with a flowing stream of water to remove excess NMP solvent. The prepared hollow fiber precursors were then deacetylated by immersion in a 0.075 M NaOH/96% ethanol solution for different times (0.5−8 h) at room temperature.

2.3. Fabrication of Hollow Fiber Carbon Membranes. The deacetylated precursors were carbonized in a tubular furnace (Carbolite HZS 12/600E) using a working tube of quartz and a quartz container, which are described elsewhere.[13] A multidwell carbonization protocol with CO_2 purge gas, a heating rate of 1 °C/min, a final temperature of 650 °C, and a soak time of 2 h was executed for the carbonization procedure. The protocol was optimized with respect to the mechanical properties of the carbon membrane and its separation properties. The first two dwells are important to remove traces of water and solvent in the precursor as shown in Figure 3. The other dwells are important to allow the carbon matrix to rearrange and form micropores between layers of graphite sheets. After the final temperature was reached, the system was allowed to cool naturally to a temperature below 50 °C before removal of the HFCMs from the furnace.

2.4. Membrane Characterization. *2.4.1. FTIR and SEM.* A Bruker Tensor 27 Fourier transform infrared (FTIR) spectrometer was used to characterize the residual acetyl content and PVP content in the deacetylated CA membranes. A Zeiss SUPRA 55VP scanning electron microscopy was used to qualitatively assess the structural and morphological characteristics of the produced HFCMs. Backscatter and secondary electron images were obtained using an acceleration potential of 5 keV. The samples measured had not been used in gas permeation tests, but were taken from the same carbonization batch as those used for the permeation test.

2.4.2. TGA and MS. The weight loss during the carbonization of the precursors was characterized by a thermogravimetric analyzer from TA Instruments (New Castle, DE), model Q500. Helium was used as the purge gas, and its flow rate was controlled at 90 mL/min. The data were processed with TA Instruments Universal Analysis 2000 software. A Thermostar gas analysis system (Pfeiffer Vacuum GmbH, Germany) was coupled to the sample gas outlet on the furnace of the TGA instrument. The mass spectrum was synchronized with the TGA results, and the data were analyzed with Quadstar TG-MS system software (TS-TAR_v7).

2.4.3. Gas Permeation Tests. The prepared HFCMs were loaded into an in-house module, and the schematic diagram of

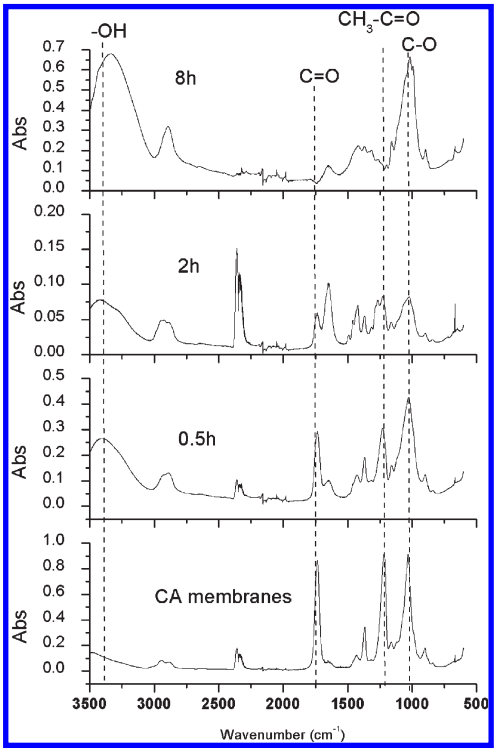

Figure 2. FTIR spectra for CA membranes and deacetylated membranes with different reaction times of 0.5, 2, and 8 h.

the module is shown in Figure 1. Single-gas permeability values were measured at 30 °C and a feed pressure of 2 bar (permeate side evacuated) in a standard pressure-rise setup (MKS Baratron pressure transducer, 0−100 mbar range) with LabView data logging. The gas permeability test setup has been described elsewhere.[13]

The order of testing was always H_2, N_2, CH_4, and finally CO_2 to prevent the strongly adsorbing gases from disturbing the performance of the more ideal or noninteracting gases in carbon membranes.[13] The tests were run from several minutes to several hours to ensure that the transient phase of diffusion was passed and a steady state had been obtained (dp/dt tends to a constant). The gas permeability, P (barrer, 1 barrer = 10^{-10} (cm^3 (STP) cm)/(cm^2 s cmHg)) can be calculated using the following equation:

$$P = \frac{(273 \times 10^7) Vl(dp/dt)}{76 \Delta p A T_{exptl}} \quad (1)$$

where V is the collection volume (cm^3) that was measured with a precalibrated permeation cell reported elsewhere,[13] dp/dt is the collection volume pressure increase rate (mbar/s), l and A are the

dx.doi.org/10.1021/ie101978q |*Ind. Eng. Chem. Res.* 2011, 50, 2080–2087

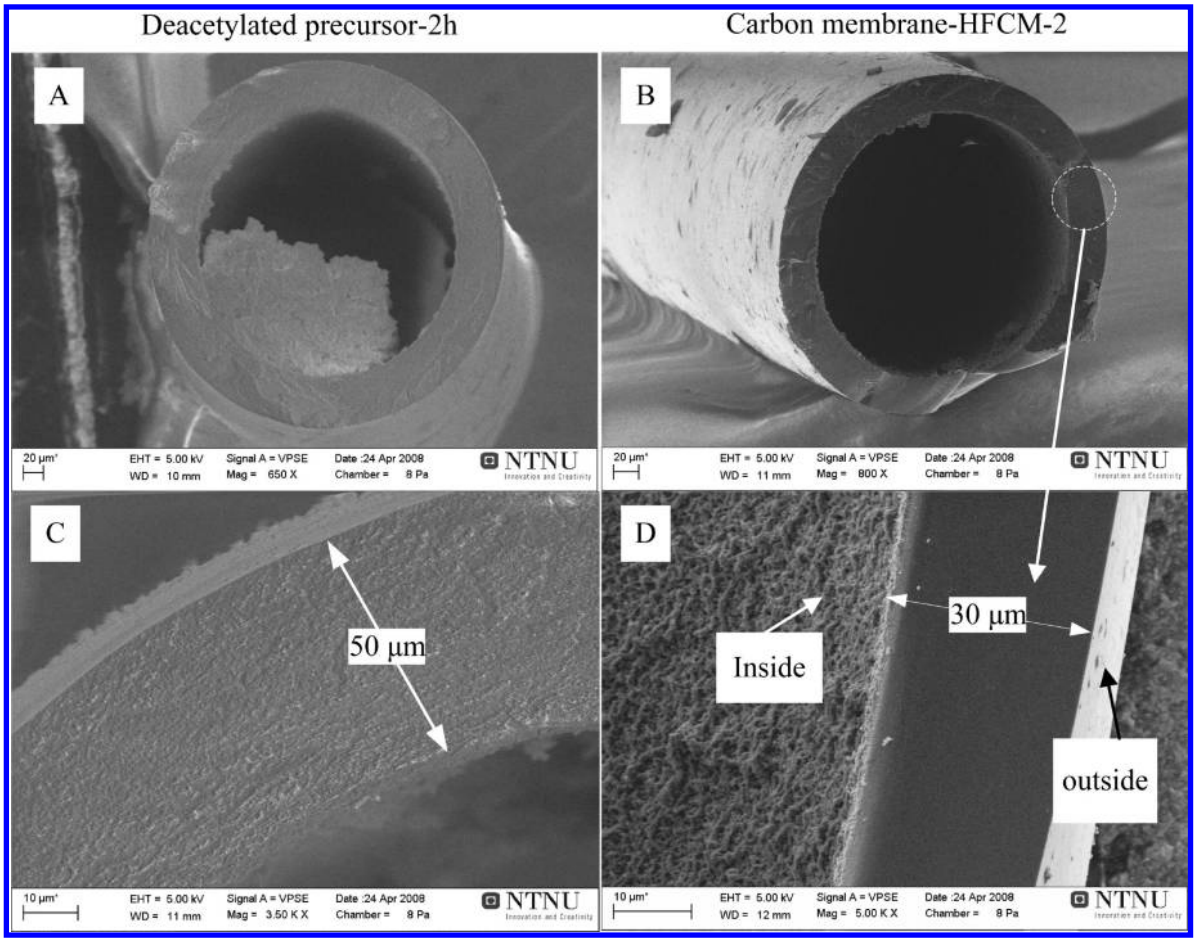

Figure 3. SEM images of the cross sections of the precursor and HFCM-2: (A, C) cross section of the precursor, (B, D) cross section of the prepared carbon membrane.

Table 1. Weight Loss for Precursor Fibers with Different Deacetylation Times

		diameter (μm)		thickness (μm)			
membrane	deacetylation time (h)	precursor	carbon membrane	precursor	carbon membrane	weight loss (%)	longitudinal shrinkage (%)
polymer membrane	0	559		93			
HFCM-0.5	0.5	430	216	65	30	78.0	37.5
HFCM-1	1	400	246	50	29	74.1	32.0
HFCM-2	2	399	250	48	30	73.5	33.3
HFCM-4	4	392	266	48	32	73.6	31.2
HFCM-8	8	390	253	48	25	74.9	32.0

thickness (cm) and total active area of the membrane sample (cm^2), respectively, ΔP (bar) is the pressure difference over the membrane, and T_{exptl} is the experimental temperature (K). In this work, the ideal selectivity is defined as the ratio of the single-gas permeabilities, which can be evaluated as follows:

$$\alpha_{A/B} = \frac{P_A}{P_B} \tag{2}$$

For gas-mixture measurements, a permeation cell and a gas chromatograph were combined to allow straightforward determination of the gas permeability. The permeation of a gas mixture containing 10% CO_2 and 90% N_2 was investigated. Considering the partial pressure of the downstream gas is relatively smaller than the upstream partial pressure, the permeability of the gas mixture in the steady state can be calculated according to the following equations:

$$P_i = \frac{(273 \times 10^7) y_i V l (dp/dt)}{76 \bar{x}_i p_H A T_{exptl}} \tag{3}$$

$$\bar{x}_i = \frac{x_{F,i} - x_{R,i}}{\ln\left(\frac{x_{F,i}}{x_{R,i}}\right)} \tag{4}$$

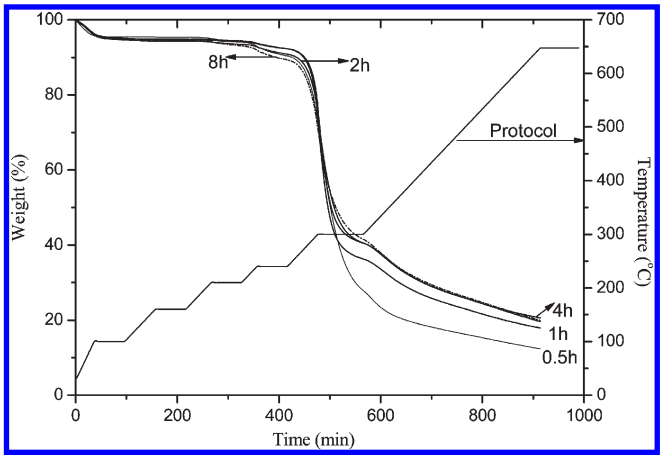

Figure 4. Carbonization procedure and weight loss of the precursor with different deacetylation times.

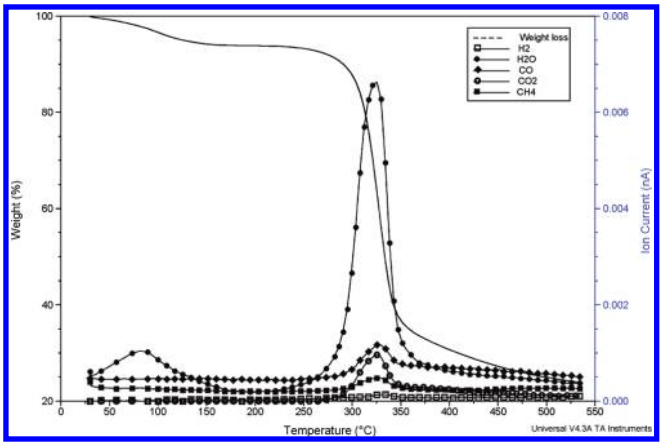

Figure 5. TGA−MS analysis for the carbonization process.

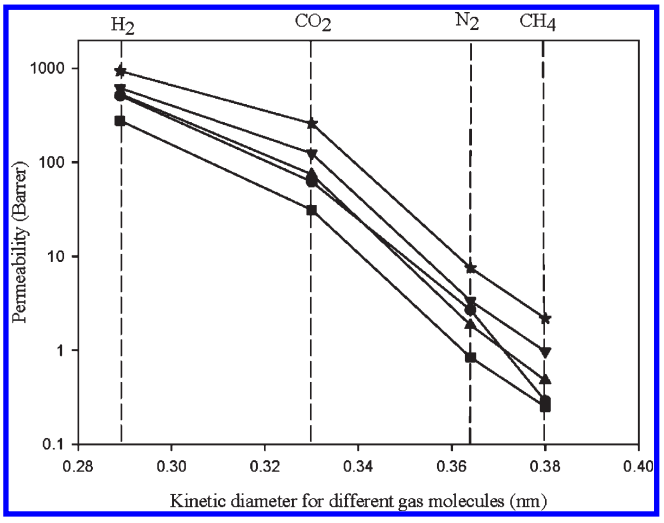

Figure 6. Single-gas permeability of (●) HFCM-0.5, (▼) HFCM-1, (+) HFCM-2, (▲) HFCM-4, and (■) HFCM-8 against the kinetic diameter of gas molecules at 303 K and 2 bar.

where P_i and p_H are the permeability of component i and the upstream pressure (bar), $x_{F,i}$ is the feed composition of component i, and $x_{R,i}$ and y_i are the molar fractions of component i in the retentate and permeate stream, respectively, which were measured by gas chromatography (GC; Agilent 6890N). The process selectivity ($S_{i/j}$) for the gas mixture was calculated using the following equation:

$$S_{i/j} = \frac{P_i}{P_j} \quad (5)$$

where P is the gas permeability as described above.

3. RESULTS AND DISCUSSION

3.1. FTIR Analysis. Figure 2 shows the FTIR spectra for the CA hollow fiber membranes and the deacetylated membranes with 0.075 M NaOH in 96% ethanol solution for different times. The peaks at 1700−1800, 1350−1400, 1200−1300, and 1000−1150 cm^{-1} attributed to the carbonyl vibration (−C═O), methyl deformations, acetyl stretching (CH_3CO-), and C−O stretching, respectively.[23] It is found that the intensities of the characteristic absorption peaks for the acetyl group (CH_3CO-) decreased following the prolonging of the reaction time, but the absorption peak at 3400 cm^{-1} (−OH) became broader as the reaction time increased compared to those of the original CA membranes. This result indicates that the number of −OH groups increases as the reaction time increases due to the conversion of cellulose acetate to cellulose gradually (CH_3CO- was substituted by −OH).

3.2. Structure and Morphology of the Precursors and HFCMs. Upon examination of the SEM images, it was concluded that the HFCMs form a symmetric structure. Figure 3 shows the cross section and inside surface of the precursors and HFCMs, respectively. The outer diameter and wall thickness of the HFCMs were approximately 250 and 30 μm, respectively, indicating a significant radical shrinkage compared to the precursor membranes with 400 and 50 μm; a typical longitudinal shrinkage of 32% was also found as shown in Table 1. This is further supported by the weight loss recorded for the hollow fibers during the carbonization process as described in section 3.2.

3.3. TGA−MS Analysis. In addition to the characterization mentioned above in section 3.1, the weight loss measurement for the pyrolysis process was carried out using TGA to mimic the carbonization conditions and hence assess the weight changes of the precursor material during the carbonization process. The weight loss of about 74% for the deacetylated CA precursors as a function of temperature was measured with TGA in a dry helium atmosphere. The weight loss is larger for short deacetylation times (<1 h) than that for longer times (>2 h), which indicates that most acetyl groups were reacted with NaOH within 2 h. To continuously prolong the deacetylation time will not change the degree of substitution for the acetyl group (DS = 1.62(acetyl content)/(43 − 0.42(acetyl content)), acetyl content (%)) significantly, as can be seen from Figure 4.

The degradation of the precursor begins at approximately 240 °C, and most of the weight loss occurs at approximately 300 °C and continues at a slower rate up to 650 °C for all precursors. Some evaporation of absorbed water was also found below 100 °C. From Figure 4, one can conclude that the carbonization protocol can be suitable for this precursor since the dwells coincide with the range of highest weight loss. The gases evolved during the carbonization were monitored using a mass spectrometer in which the dry helium swept the gas residue into the mass spectrometer (at a flow rate of 90 mL/min). The acquired information is plotted against the weight loss of the precursor

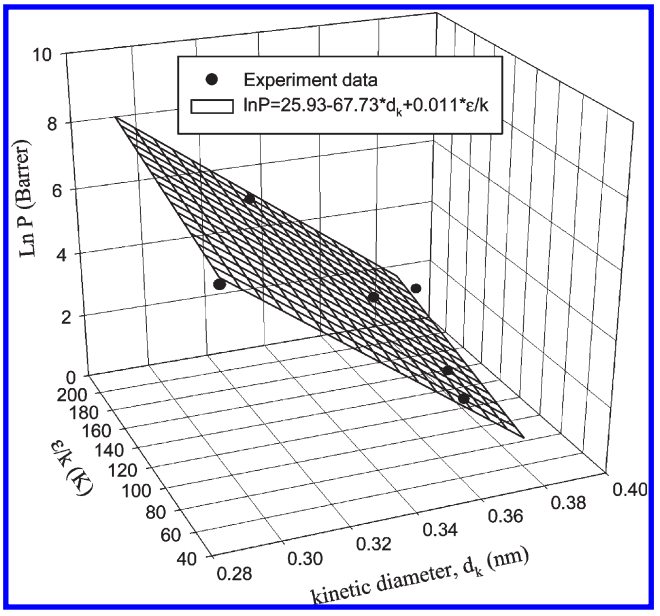

Figure 7. Permeability versus kinetic diameter and Lennard-Jones well depth.

with a deacetylation time of 2 h in Figure 5. Wu et al. reported that the cellulose carbonization generates H_2, CO_2, CO, H_2O, CH_4, and other volatiles.[24] In this work, the onset of large weight loss coincided with the increase of H_2, CO_2, CO, H_2O, CH_4, and so on. The main MS peak of H_2O occurs around 290−350 °C, indicating that water is evolved mostly via the chemical dehydration because the physical adsorbed water has been greatly removed in the predrying process (<200 °C) on the basis of TGA−MS detection. Therefore, the carbonization mechanism is possibly dominated by the dehydration reaction. The thermal cleavages of C−O and C−C linkages can result in the formation of CO and CO_2. Following the ring opening, the volatiles of the evolution are further eliminated from the glycoside links of the deacetylated cellulose acetate, which can accelerate the conversion from the cellulosic structure to the turbostratic carbon structure that will greatly affect the performance of the resulting hollow fiber carbon membranes.

3.4. Gas Separation Properties. *3.3.1. Single-Gas Tests.* Figure 6 illustrates the gas permeability values of H_2, CO_2, N_2, and CH_4 versus the gas molecule kinetic diameters for the prepared HFCMs with different deacetylation times. HFCM-2 with the optimal deacetylation time of 2 h shows the highest permeability for the tested gas molecules. The gas permeability values of the selected gases were found to be in the following order: H_2 (2.89 Å) > CO_2 (3.3 Å) > N_2 (3.64 Å) > CH_4 (3.8 Å). The permeability values decrease with increasing kinetic diameter of the gases, indicating that the main transport mechanism of HFCMs is molecular sieving. The most popular approach to linking porosity complexity to intraparticle diffusional behavior is via the so-called tortuosity factor. Thus, for a sample of a porous material, an effective diffusivity is defined as[25]

$$D_e = \frac{\varepsilon_p}{\tau} D \tag{6}$$

where D_e is the effective diffusion coefficient and ε_p and τ represent the microporosity and tortuosity factor, respectively, for carbon membranes. Therefore, the flux for component i (J_i) can

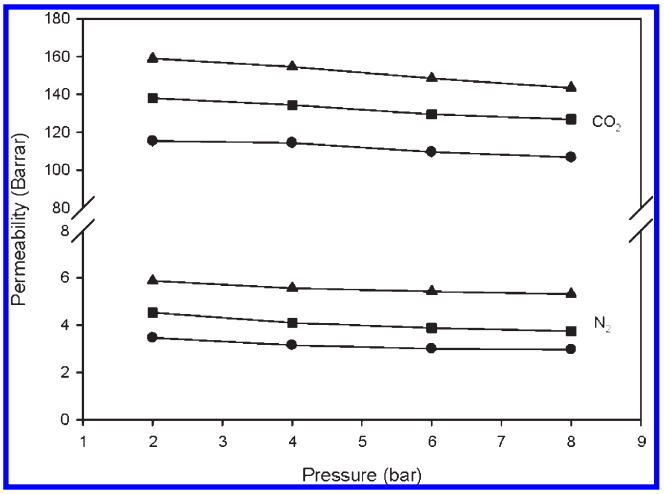

Figure 8. Effects of the temperature and pressure on the gas permeability for HFCM-2: (●) 30 °C, (■) 50 °C , (▲) 70 °C.

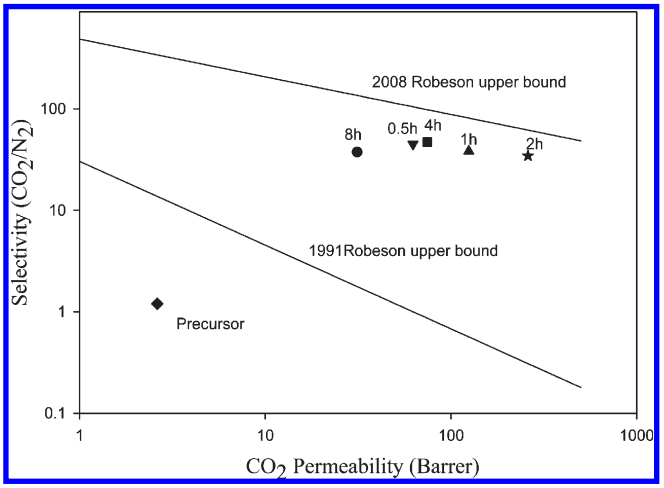

Figure 9. Separation performance for the CO_2/N_2 pair at 30 °C and 2 bar.

be described as follows:[26]

$$J_i = \frac{\varepsilon_p \Delta p}{\tau \mathrm{RTL}} D_0 \exp\left(\frac{-E_{a,i}}{RT}\right) \tag{7}$$

Here $E_{a,i}$ is the activation energy for diffusion in the molecular sieving process for HFCMs, and D_0 may be expressed as[27]

$$D_0 = e\lambda^2 \frac{kT}{h} \exp\left(\frac{S_a}{R}\right) \tag{8}$$

Combining eqs 7 and 8, the permeability can be calculated by

$$P_i = \frac{\varepsilon_p e\lambda^2 k}{\tau \mathrm{Rh}} \exp\left(\frac{S_a}{R}\right) \exp\left(\frac{-E_{a,i}}{RT}\right) \tag{9}$$

Suda et al. reported that the activation energy and activation entropy were correlated linearly with the kinetic diameter, d_k, and Lennard-Jones well depth, ε/k^2. Therefore, we assumed

$$E_a = a_1 d_k + b_1 \qquad S_a = a_2 e/k + b_2 \tag{10}$$

dx.doi.org/10.1021/ie101978q |*Ind. Eng. Chem. Res.* 2011, 50, 2080–2087

Substituting eq 10 into eq 9 and taking the logarithm of both sides, eq 9 can be modified as

$$\ln P = c + \frac{-a_1}{RT} d_k + \frac{a_2}{R} e/k \qquad (11)$$

where a_1, a_2, and c are constants. Keeping the temperature constant (303 K), and plotting ln P versus d_k and ε/k, the corresponding result for HFCM-2 is shown in Figure 7. The following regression equation was obtained on the basis of the experiment data:

$$\ln P = 25.93 - 67.73 d_k + 0.011 \varepsilon/k \qquad (12)$$

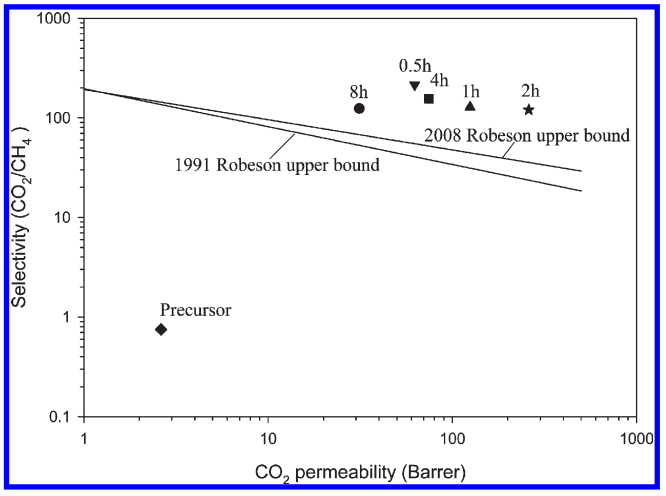

Figure 10. Separation performance for the CO_2/CH_4 pair at 30 °C and 2 bar.

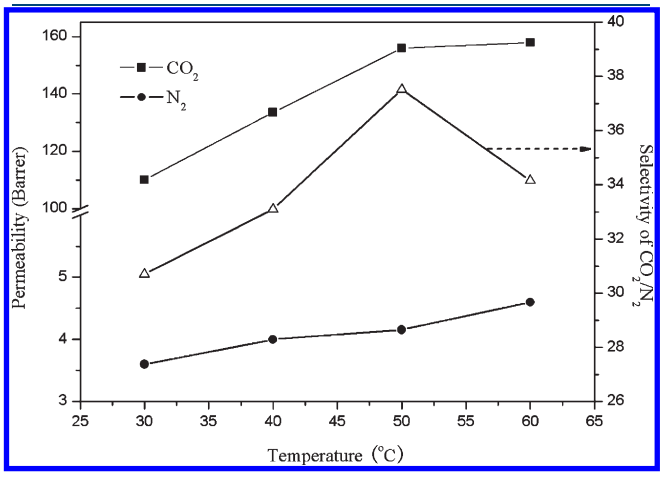

Figure 11. Dependency of the gas permeability and selectivity on the temperature for the gas-mixture test at 303 K and a feed flow rate of 10 mL/min.

The negative coefficient of the parameter d_k represents that the larger gas molecule kinetic diameter has a lower permeability through this carbon membrane. Moreover, eq 12 also indicates that the kinetic diameter is more important due to the larger absolute value compared to the Lennard-Jones well depth, which means that diffusion is dominated by a molecular sieving process and sorption has a relatively small influence.

To investigate the effects of the temperature and pressure on the gas separation performance, the permeability values of CO_2 and N_2 for HFCM-2 were tested at different temperatures (30−70 °C) and pressures (2−8 bar) as shown in Figure 8. As expected from eq 8, an increase of temperature leads to a higher permeability for both CO_2 and N_2 in this narrow temperature range. The effect of pressure on the permeability in the range studied can be neglected as shown in the figure. This is basically due to the rigid structure of carbon membranes. Figures 9 and 10 give the permeability and ideal selectivity of CO_2/N_2 and CO_2/CH_4 for the carbon membranes prepared from precursors with different deacetylation times. On the basis of the Robeson upper bound as published in 1991 and 2008,[28,29] the hollow fiber carbon membranes exhibit great gas permeability and selectivity properties compared to the precursors and most polymeric membranes.

3.3.2. Gas-Mixture Measurements. Single-gas permeation properties are usually used as the basic results to indicate the ideal separation performance of carbon membranes. However, the separation properties are affected by the presence of other penetrants in a gas mixture. The transport of a component in a gas mixture through membranes is different from that obtained from the single-gas measurement, especially in the separation of absorbable gas, i.e., CO_2. The adsorption of gas molecules in a carbon matrix will significantly affect the other less or nonabsorbable gas molecules (e.g., N_2). Figure 11 shows the dependency of the gas separation properties for HFCM-2 on the temperature with a constant feed pressure and flow rate of 3.5 bar and 10 mL/min, respectively. This figure indicates the difference in temperature dependency for the two gases CO_2 and N_2. The permeability for both will increase with increasing temperature up to 50 °C, while in the range 50−60 °C the difference in nonideal versus ideal properties is clearly shown and the selectivity goes down. This is usually true for most gas mixtures containing both nonideal and ideal gases. A sensitivity analysis should therefore be performed to find the optimum temperature conditions for the separation of a given gas mixture. Table 2 gives the comparison of the gas separation performance for single-gas and gas-mixture tests at different temperatures. The permeability of N_2 in the mixture is lower than that of the single-gas results, which indicates the presence of competing transport in the mixture. The selectivity of CO_2/N_2 in the gas mixture is higher than that of single gases since the adsorbed gas CO_2 in the pores will hinder the transport of nonadsorbable and ideal N_2.

Table 2. Comparison of Carbon Membrane Performances between Single-Gas and Gas-Mixture Tests

		gas mixture (10%/90% CO_2/N_2)					single gas (p_{CO_2} = 0.35 bar, p_{N_2} = 3.15 bar)		
membrane	temp (°C)	feed pressure (bar)	stage-cut (%)	process selectivity (CO_2/N_2)	CO_2 perm[a] (barrer)	N_2 perm[a] (barrer)	ideal selectivity (CO_2/N_2)	CO_2 perm[a] (barrer)	N_2 perm[a] (barrer)
HFCM-2	30	3.5	1.0	30.7	110.0	3.6	13.2	134.5	10.2
	50	3.5	1.1	37.5	156.0	4.2	15.3	162.6	10.6

[a] The abbreviation "perm" represents permeability.

dx.doi.org/10.1021/ie101978q |*Ind. Eng. Chem. Res.* 2011, 50, 2080–2087

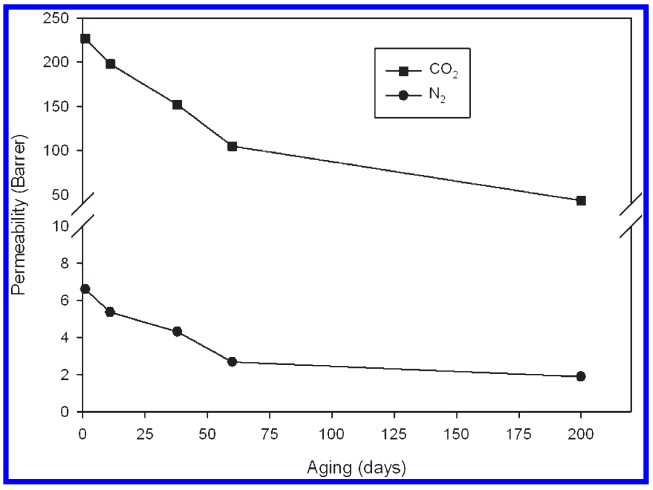

Figure 12. Aging of HFCM-2 by exposure to the laboratory atmosphere at room temperature.

3.3.3. Aging test. A challenge for most membranes is often the lack of long-term stability; this relates to both organic (polymeric) and inorganic (ceramic, CMS) membranes. To investigate the durability of a carbon membrane, long-term stability (aging) tests were conducted. HFCM-2 was statically exposed to the laboratory air (i.e., not in any way protected over time), and Figure 12 shows the aging test results. From this figure, we find that the permeability values decreased for both gases over ~7 months, especially for CO_2. No regeneration was performed during this time. The aging may be caused by the chemisorption of O_2 into the carbon matrix when exposed to air. Some regeneration methods such as thermal, chemical, and electrothermal techniques have been investigated by several groups;[30−32] these are not discussed here.

4. CONCLUSIONS

HFCMs were prepared from deacetylated CA precursors by controlling a multidwell carbonization protocol with CO_2 purge gas, a heating rate of 1 °C/min, a final thermal temperature of 650 °C, and a soak time of 2 h. Different performance carbon membranes can be prepared from the precursors with various deacetylation times under the same carbonization procedure. HFCM-2 was fabricated from the precursor with the optimal deacetylation time of 2 h and showed the best permeability for the tested gas molecules. The permeation properties of the prepared HFCMs for different gases, H_2, CO_2, N_2, and CH_4, were in accordance with the kinetic diameters of the gas molecules (<4 Å), which indicated that the molecular sieving mechanism dominated the transport process. The results also showed that the kinetic diameter has a larger effect than the Lennard-Jones well depth, which indicates that the diffusion is dominated by a molecular sieving process and that the sorption has a relatively small influence. The single gas indicated that the permeability increased with temperature and was mostly independent of the feed gas pressure due to the rigid structures of the carbon membranes. The gas-mixture test indicates that the permeability and selectivity should be optimized for the specific carbon membrane separation process. The aging test result indicates that the permeability of the carbon membrane will decrease over time when it is exposed to the laboratory air.

AUTHOR INFORMATION

Corresponding Author

*Tel.: +47 73594033. Fax: +47 73594080. E-mail: may-britt.hagg@chemeng.ntnu.no.

ACKNOWLEDGMENT

We acknowledge the NanoGloWa project for funding (EU's 6th framework program) of the current work.

NOMENCLATURE

a, b, c = constants
A = effective membrane area, cm^2
d = kinetic diameter, nm
D = diffusion coefficient, $m^2\ s^{-1}$
e = electron charge, 1.602×10^{-19} C
E = activation energy, J
h = Planck constant, 6.626×10^{-34} J s
J = flux, mol $m^{-2}\ s^{-1}$
k = Boltzmann constant, 1.381×10^{-23} J K^{-1}
l = effective membrane thickness, μm
P = permeability, barrer
p = pressure, bar
R = molar gas constant, 8.314 J K^{-1} mol^{-1}
S = entropy, J K^{-1}, and selectivity
t = time, s
T = temperature, K
V = volume, cm^3
x = mole composition
y = mole composiiton

Subscripts

A = compound A
a = activation
B = compound B
e = effective
F = feed
H = upstream
i = ith component
j = jth component
k = kinetic
R = retentate

Greek Letters

α = selectivity
ε = microporosity and Lennard-Jones well depth
λ = mean free path, m
τ = tortuosity

REFERENCES

(1) Fuertes, A. B.; Centeno, T. A. Preparation of supported asymmetric carbon molecular sieve membranes. *J. Membr. Sci.* **1998**, *144* (1−2), 105–111.

(2) Suda, H.; Haraya, K. Gas permeation through micropores of carbon molecular sieve membranes derived from Kapton polyimide. *J. Phys. Chem. B* **1997**, *101* (20), 3988–3994.

(3) Steel, K. M.; Koros, W. J. Investigation of porosity of carbon materials and related effects on gas separation properties. *Carbon* **2003**, *41* (2), 253–266.

(4) Barsema, J. N.; van der Vegt, N. F. A.; Koops, G. H.; Wessling, M. Ag-functionalized carbon molecular-sieve membranes based on polyelectrolyte/polyimide blend precursors. *Adv. Funct. Mater.* **2005**, *15* (1), 69–75.

(5) David, L. I. B.; Ismail, A. F. Influence of the thermastabilization process and soak time during pyrolysis process on the polyacrylonitrile carbon membranes for O_2/N_2 separation. *J. Membr. Sci.* **2003**, *213* (1−2), 285–291.

(6) Zhou, W.; Yoshino, M.; Kita, H.; Okamoto, K.-i. Carbon molecular sieve membranes derived from phenolic resin with a pendant sulfonic acid group. *Ind. Eng. Chem. Res.* **2001**, *40* (22), 4801–4807.

(7) Zhang, B.; Wang, T.; Zhang, S.; Qiu, J.; Jian, X. Preparation and characterization of carbon membranes made from poly(phthalazinone ether sulfone ketone). *Carbon* **2006**, *44* (13), 2764–2769.

(8) Yoshimune, M.; Fujiwara, I.; Haraya, K. Carbon molecular sieve membranes derived from trimethylsilyl substituted poly(phenylene oxide) for gas separation. *Carbon* **2007**, *45* (3), 553–560.

(9) Lee, H.-J.; Suda, H.; Haraya, K.; Moon, S.-H. Gas permeation properties of carbon molecular sieving membranes derived from the polymer blend of polyphenylene oxide (PPO)/polyvinylpyrrolidone (PVP). *J. Membr. Sci.* **2007**, *296* (1−2), 139–146.

(10) Campo, M. C.; Magalhães, F. D.; Mendes, A. Carbon molecular sieve membranes from cellophane paper. *J. Membr. Sci.* **2010**, *350* (1−2), 180–188.

(11) Barsema, J. N. Carbon membranes: Precursor, preparation and functionalization. Ph.D. Thesis, University of Twente, Enschede, The Netherlands, 2007.

(12) Favvas, E. P.; Kapantaidakis, G. C.; Nolan, J. W.; Mitropoulos, A. C.; Kanellopoulos, N. K. Preparation, characterization and gas permeation properties of carbon hollow fiber membranes based on Matrimid(R) 5218 precursor. *J. Mater. Process. Technol.* **2007**, *186* (1−3), 102–110.

(13) Lie, J. A. Synthesis, performance and regeneration of carbon membranes for biogas upgrading—A future energy carrier. Ph.D. Thesis, Norwegian University of Science and Technology, Trondheim, Norway, 2005.

(14) Saufi, S. M.; Ismail, A. F. Development and characterization of oolyacrylonitrile (PAN) based carbon hollow fiber membrane. *Songklanakarin J. Sci. Technol.* **2002**, *24* (Suppl.), 843–854.

(15) Vu, D. Q.; Koros, W. J.; Miller, S. J. Effect of condensable impurities in CO_2/CH_4 gas feeds on carbon molecular sieve hollow-fiber membranes. *Ind. Eng. Chem. Res.* **2003**, *42* (5), 1064–1075.

(16) Vu, D. Q.; Koros, W. J.; Miller, S. J. High pressure CO_2/CH_4 separation using carbon molecular sieve hollow fiber membranes. *Ind. Eng. Chem. Res.* **2001**, *41* (3), 367–380.

(17) He, X.; Lie, J. A.; Sheridan, E.; Hägg, M.-B. Preparation and characterization of hollow fibre carbon membranes based on a cellulosic precursor. Presented at ICOM 2008, Honolulu, HI, 2008.

(18) He, X.; Lie, J. A.; Sheridan, E.; Hägg, M.-B. CO_2 Capture by hollow fibre carbon membranes: Experiments and process simulations. Presented at GHGT-9, Washington, DC, 2008.

(19) Chung, T. S.; Hu, X. Effect of air-gap distance on the morphology and thermal properties of polyethersulfone hollow fibers. *J. Appl. Polym. Sci.* **1997**, *66*, 1067.

(20) Qin, J.-J.; Li, Y.; Lee, L.-S.; Lee, H. Cellulose acetate hollow fiber ultrafiltration membranes made from CA/PVP 360 K/NMP/water. *J. Membr. Sci.* **2003**, *218* (1−2), 173–183.

(21) Liu, H.; Hsieh, Y.-L. Ultrafine fibrous cellulose membranes from electrospinning of cellulose acetate. *J. Polym. Sci., Part B: Polym. Phys.* **2002**, *40* (18), 2119–2129.

(22) Son, W. K.; Youk, J. H.; Lee, T. S.; Park, W. H. Electrospinning of ultrafine cellulose acetate fibers: Studies of a new solvent system and deacetylation of ultrafine cellulose acetate fibers. *J. Polym. Sci., Part B: Polym. Phys.* **2004**, *42*, 5–11.

(23) Kang, K. S.; Cho, K. Y.; Lim, H. K.; Kim, J. Investigation of surface morphology of cellulose acetate micro-mould after deacetylation. *J. Phys. D: Appl. Phys.* **2008**, *41*, 195403.

(24) Wu, Q.; Pan, N.; Deng, K.; Pan, D. Thermogravimetry−mass spectrometry on the pyrolysis process of Lyocell fibers with and without catalyst. *Carbohydr. Polym.* **2008**, *72* (2), 222–228.

(25) Prachayawarakorn, S.; Mann, R. Effects of pore assembly architecture on catalyst particle tortuosity and reaction effectiveness. *Catal. Today* **2007**, *128* (1−2), 88–99.

(26) Hagg, M.-B.; Lie, J. A.; Lindbrathen, A. Carbon molecular sieve membranes. A promising alternative for selected industrial applications. *Ann. N.Y. Acad. Sci.* **2003**, *984* (1), 329–345.

(27) Glasstone, S.; Laidler, K. J.; Eyring, H. *The Theory of Rate Processes*, 1st ed.; McGraw-Hill Book Co.: New York, 1941.

(28) Robeson, L. M. Correlation of separation factor versus permeability for polymeric membranes. *J. Membr. Sci.* **1991**, *62* (2), 165–185.

(29) Robeson, L. M. The upper bound revisited. *J. Membr. Sci.* **2008**, *320* (1−2), 390–400.

(30) Jones, C. W.; Koros, W. J. Carbon molecular sieve gas separation membranes—II. Regeneration following organic exposure. *Carbon* **1994**, *32* (8), 1427–1432.

(31) Menendez, I.; Fuertes, A. B. Aging of carbon membranes under different environments. *Carbon* **2001**, *39* (5), 733–740.

(32) Lie, J. A.; Hagg, M.-B. Carbon membranes from cellulose: Synthesis, performance and regeneration. *J. Membr. Sci.* **2006**, *284* (1−2), 79–86.